Journal of Hazardous Materials 312 (2016) 234–242

Contents lists available at ScienceDirect

Journal of Hazardous Materials

journal homepage: www.elsevier.com/locate/jhazmat

Aging study on carboxymethyl cellulose-coated zero-valent iron nanoparticles in water: Chemical transformation and structural evolution

Haoran Dong[a,b,*], Feng Zhao[a,b], Guangming Zeng[a,b], Lin Tang[a,b], Changzheng Fan[a,b], Lihua Zhang[a,b], Yalan Zeng[a,b], Qi He[a,b], Yankai Xie[a,b], Yanan Wu[a,b]

[a] College of Environmental Science and Engineering, Hunan University, Changsha, Hunan 410082, China
[b] Key Laboratory of Environmental Biology and Pollution Control (Hunan University), Ministry of Education, Changsha, Hunan 410082, China

HIGHLIGHTS

- The chemical transformation and structural evolution of CMC-nZVI were investigated.
- CMC could slow down the aging rate of nZVI and alter the species transformation.
- Fe_3O_4 and/or γ-Fe_2O_3 are the dominant corrosion products of bare nZVI after aging.
- γ-FeOOH is the primary corrosion product of CMC-nZVI after aging.

GRAPHICAL ABSTRACT

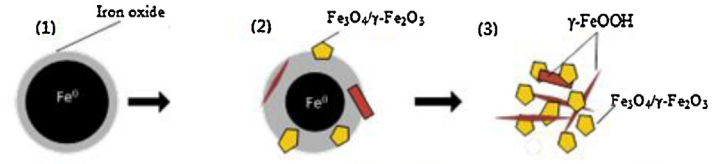

Bare nZVI: (1) Fresh; (2) Short-term aging (5-15 d); (3) Long-term aging (30-90 d)

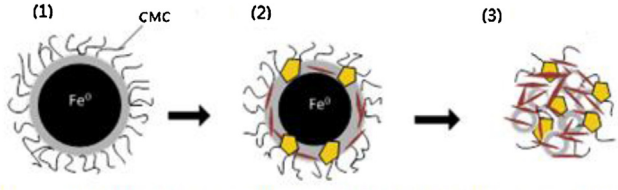

CMC-nZVI: (1) Fresh; (2) Short-term aging (5-15 d); (3) Long-term aging (30-90 d)

ARTICLE INFO

Article history:
Received 9 February 2016
Received in revised form 24 March 2016
Accepted 25 March 2016
Available online 26 March 2016

Keywords:
Aging
Chemical transformation
Composition evolution
Characterization
Nanoscale zero-valent iron

ABSTRACT

To assess the long-term fate and the associated risks of nanoscale zero-valent iron (nZVI) used in the water remediation, it is essential to understand the chemical transformations during aging of nZVI in water. This study investigated the compositional and structural evolution of bare nZVI and carboxymethyl cellulose (CMC) coated nZVI in static water over a period of 90 days. Fourier transform infrared spectroscopy (FTIR), Scanning electron microscopy (SEM), X-ray diffraction (XRD) and Raman spectroscopy were used to characterize the corrosion products of nZVI and CMC-nZVI. Results show that both the structures and the compositions of the corrosion products change with the process of aging, but the coating of CMC could slow down the aging rate of nZVI (as indicated by the slower drop in Fe^0 intensity in XRD pattern). For the bare nZVI, magnetite (Fe_3O_4) and/or maghemite (γ-Fe_2O_3) are the dominant corrosion products after 90 days of aging. However, for the CMC-nZVI, the core-shell spheres collapses to acicular-shaped structures after aging with crystalline lepidocrocite (γ-FeOOH) as the primary end product. Moreover,

* Corresponding author at: College of Environmental Science and Engineering, Hunan University, Changsha, Hunan 410082, China.
E-mail address: dongh@hnu.edu.cn (H. Dong).

http://dx.doi.org/10.1016/j.jhazmat.2016.03.069

more lepidocrocite present in the corrosion products of CMC-nZVI with higher loading of CMC, which reveals that the CMC coating could influence the transformation of iron oxides.

1. Introduction

Iron nanoparticle technology has been considered to be one of the first generation of nanoscale environmental technologies [1]. Substantial researches have demonstrated nanoscale zero-valent iron (nZVI) have large specific surface area and high surface reactivity relevant its core-shell structure with a zero-valent iron core surrounded by an iron oxide/hydroxide layer [2,3]. This material has been used to degrade a wide range of organic and inorganic soil and water contaminants [4–10].

nZVI particles naturally oxidize upon reaction with water and oxygen resulting in a significant decrease in reactivity [11]. The formation of different mineral phases on the particle surface, which may occur within the desired functional lifetime of nZVI particles, affects the reactivity, hydrodynamics, and mobility of nZVI in the environment [12]. Therefore, it is important to understand the transformation of nZVI particles during long-term water exposure.

Previous studies showed that fresh nZVI consists of a Fe^0 core surrounded by an oxide shell with a near-perfect spherical shape [2]. The structure, shape, and composition of nZVI change with time upon exposure to water. Long-term aging leads to the formation of lepidocrocite and magnetite/maghemite [11,13–15]. Different morphologies and compositions have been observed when iron nanoparticles are oxidized, ranging from iron/iron oxide core-shell structures [16] to iron/iron oxide core-void-shell structures, iron oxide solid spheres, or even iron-based hollow structures [17,18]. It has reported that the structure and composition of aged nZVI varied considerably, depending on the iron types (e.g., $Fe^H{}_2$, produced by the hydrogen reduction of ferric oxides and Fe^{BH}, prepared using a borohydride reduction method), solution composition, solution pH, DO, temperature, and so on [19–21].

Phenrat et al. [22] has shown that bare (unmodified) nZVI particles can aggregate very rapidly because of attractive magnetic forces. To increase the stability and mobility of nZVI for engineering application, various modification approaches have been attempted, such as bimetallic system [23], carboxymethyl cellulose (CMC) [24–27], guar gum [28], polyacrylic acid [27,29,30] and surfactant [31,32] modification. Until now, the corrosion of bare nZVI during longtime water exposure has been widely reported [11,15,20]; however, the structural characteristics and evolution process of the engineered modified nZVI particles with surface coatings have not been systematically investigated. This information would be of great importance for the understanding of the long-term fate of surface-modified nZVI in the water environment and the risk assessment for the use of the engineered nZVI particles in subsurface remediation.

The overall objective of this study is to investigate the structural and compositional evolution of nZVI modified with carboxymethyl cellulose (CMC) in static aquatic media over a period of 90 days. CMC is a polyelectrolyte and carries carboxylate groups in addition to hydroxyl groups. Previous studies have shown that CMC strongly interact with nZVI particles and stabilize the nanoparticles effectively [24]. Morphological and mineralogical characteristics of bare nZVI and nZVI modified with CMC in various stages of aging are studied by Fourier transform infrared spectroscopy (FTIR), scanning electron microscope (SEM), X-ray diffraction (XRD) and Raman spectroscopy.

2. Experimental methods

2.1. Materials and chemicals

Carboxymethyl cellulose (CMC, MW = 90,000) were purchased from Jingkang new material technology co. (Changsha). nZVI particles (Nanofer 25, produced from nanosized ferrihydrite) in aqueous dispersion form were graciously supplied by the NANOIRON® Company (Czech Republic, EU). All reagents for experiments were of reagent grade and used without further purification. All solutions and dilutions were prepared in ultrapure water (Barnstead D11911).

2.2. Preparation of iron nanoparticles

A stock suspension of Nanofer 25 of 200 g L^{-1} (referred to as nZVI in this study) was prepared. Suspensions of nZVI (500 mg L^{-1}) were prepared by dilution with stock suspension in N_2-purged water under neutral conditions (pH ~ 7). The solution pH was measured by a pH meter (INESA, PHS-3C). The pure CMC solutions were prepared and homogenized overnight using magnetic stirrers to ensure complete hydration and dissolution [33]. The CMC-coated nZVI (CMC-nZVI) was synthesized by dispersing nZVI particles in aqueous CMC to result in suspensions, comprising iron nanoparticles (500 mg L^{-1}) and CMC of various concentrations (0.2, 0.4, 0.6, 0.8, 1.0, 1.2, 1.4 and 1.6 wt%) individually. The particle suspensions were then ultrasonicated for 30 min to complete the formation of CMC-nZVI.

2.3. Sedimentation and aging experiments

A sedimentation assessment of the CMC-nZVI suspensions was then performed to determine the stabilizer concentration for the efficient stabilization. Digital photographs of the vials containing CMC-nZVI suspensions were taken up to 60 min to qualitatively assess the rate of sedimentation and nanoparticle stability by observing the turbidity of the suspension (Fig. S1 in the supporting information (SI)). The bare and CMC-nZVI nanoparticles showed different sedimentation behavior. The iron nanoparticles rapidly settled within 60 min. CMC-nZVI deposited less when the concentration of CMC increased from 0.2 wt% to 1.6 wt%. The sedimentation kinetics of CMC-nZVI with different CMC loadings (0.4, 0.8, 1.2, 1.6 wt%) was further determined quantitatively by monitoring the optical absorbance at 508 nm by UV–vis spectrophotometery (UV-2550, SHIMADZU, Japan) in a drive-time mode for 1 h. CMC-nZVI coated with 0.4 wt% (less efficient stabilization) and 1.2 wt% (efficient stabilization) were employed in the subsequent aging experiments to examine the effect of CMC concentration on nZVI corrosion. The solid samples were filtered and collected after 0, 5, 15, 30, 60, and 90 days of aging. The experiments were carried out in static water (40 mL) in an open vial (50 mL), which represents the static aquatic media exposed to the air. All measurements were made at 25 °C in duplicate.

2.4. Characterization of fresh and aged iron nanoparticles

The collected solid samples of bare nZVI and CMC-nZVI at various aging states were freeze-dried before further analyses by FTIR,

SEM, XRD and Raman spectroscopy. FTIR (Magna-IR 750, Nicolet) measurements were carried out to explore the modes of interactions between CMC and the nanoparticle surface. SEM (FEI QuANTA 200, Czech) was used to characterize the structure and morphologies of the iron nanoparticles. XRD analyses were operated with a Rigaku D/Max 2500 with Cu-Kα radiation at 40 kV/250 mA. Raman spectra are obtained with a Labram-010 from France with a 632 nm laser. Spectra were collected over the range 4000–40 cm^{-1}.

3. Results and discussion

3.1. Stability behavior of bare nZVI and CMC-nZVI

To compare the colloidal stability of the different nanoparticles, sedimentation tests were performed at a particle concentration of 500 mg L^{-1}. CMC molecules can be adsorbed onto the surface of nZVI nanoparticles, resulting in a layer of physical barrier and negative charges and thereby preventing the nanoparticles from agglomeration [34]. The concentration of CMC in the suspension is expected to affect the growth and aggregation of nZVI particles. The data shown in Fig. 1 bring insight into the effect of CMC on nZVI deposition kinetics. UV–vis measurements were taken for CMC-nZVI with different CMC loadings to assess the colloidal stability of CMC-nZVI within 1 h. Greater absorbance reduction represents more serious sediment of nanoparticles after 1 h and vice versa represents the better suspension performance of the nanoparticles. In vials containing a suspension of bare nZVI, the absorbance at 508 nm was reduced by almost 80% of the initial absorbance in 1 h under quiescent conditions. Much of this change in absorbance should be attributable to the rapid settling of colloidally unstable bare nZVI. In comparison, the absorbance of CMC-nZVI was reduced by only about 40%–10% with increasing CMC concentration from 0.4 wt% to 1.6 wt% over 1 h. The suspension stability was consistent with others as reported in the literature [25,35]. The changes in absorbance in these systems were attributed to the aggregation of the particles, which led to fewer but larger particles and altered light transmittance through the suspension [33,36]. Bare nZVI aggregated and settled out of the supernatant rapidly because its larger particle size contributes to the higher magnetic and van der Waals attractive forces between particles and it has low surface charge that does not provide significant electrostatic stabilization [37]. However, the CMC coating can slow down the deposition of the nanoparticles by reducing the magnetic attraction of the iron nanoparticles to each other due to repulsion effect.

3.2. FTIR analysis

To elucidate the stabilization mechanisms and gain further insight into the interactions between the various functional groups of CMC and the nanoparticles, FTIR measurements were carried out on CMC and the 0.4 wt% CMC-stabilized nanoparticles. Fig. 2 compares the characteristic stretching frequencies of CMC alone and 0.4 wt% CMC-stabilized iron nanoparticles at various aging states and Table 1 gives the assignments of the peaks. If CMC molecules are adsorbed onto the surface of the iron nanoparticles, the stretching frequencies for the functional groups of CMC are expected to shift. It can be observed from the graph that the fresh and aged samples show IR band changes related to the complexation sites (—COO group, bands 3 and 4 in Table 1). It is proposed that Fe formed strongly-bound inner-sphere complex with the carboxyl group of CMC as —COOFe. The —OH stretching band shifts from 3441 cm^{-1} for CMC to 3415 cm^{-1} for the fresh and aged CMC-nZVI particles. This observation indicates that an enhanced intermolecular hydrogen bond is formed between CMC and the Fe particle surface [34]. Given the abundance of —OH groups in CMC, this type of hydrogen bonding can be important in binding CMC to the Fe nanoparticles, although the individual bond strength might not be as strong as that between nZVI and the carboxyl groups. Moreover, the band assigned to CH_2 stretch (Band 2) showed apparent switches (the band disappeared in the fresh and aged CMC-nZVI), resulting from the interaction between CMC and nZVI. After aging from 5 days to 90 days, the peak of CMC-nZVI almost had no change, which shows that the CMC groups remain invariant during the aging process. It can also be concluded that the aging process makes insignificant impact on the interaction between CMC and nZVI.

Table 1
FTIR peak assignments for CMC and 0.4 wt% CMC-nZVI.

Band number	Peak position (cm^{-1})		Assignments
	CMC	CMC-nZVI	
Band 1	3441	3415	O—H stretch
Band 2	2922	Disappeared	Asymmetric CH_2 stretch
Band 3	1616	1632	COO— (asymmetric)
Band 4	1423	1411	COO— (symmetric) and —CH_2 scissoring
Band 5	1148	1142	C—O—C stretch (RCH_2OCH_2R)
Band 6	1053	Disappeared	C—O stretch (RCH_2OH)

3.3. SEM analysis

Representative SEM images illustrate the particle size and morphology of fresh and aged iron nanoparticles (nZVI and 0.4 wt% CMC-nZVI) are shown in Fig. 3. The fresh nZVI particles are generally spherical in shape with the majority in the size range of nanoscale. A close-up image (Fig. 3a) reveals that the particles are connected in chains due to magnetic dipole interactions and aggregation [11]. After 5 days of aging, many flaky minerals are observed with some oxidized particles remaining (Fig. 3b). Liu et al. [11] observed a loss of the Fe(0) core and the appearance of hollowed-out oxide shells during aging. This oxidation behavior is evidence that under oxygenated aqueous conditions, oxidation occurs at the oxide-water interface as a result of the outward diffusion of iron ions from the nZVI core and formation of a new oxide phase on the particle surface [11]. Outward diffusion of iron ions has also been observed for the oxidation of iron nanoparticles in the presence of oxygen [17,38]. When the aging time reaches 15 days and 30 days, the structure of nZVI particles are partly transformed to rod-like substances (Fig. 3c and d). When the aging time is increased to 60 days and 90 days, some needle-shaped minerals are noticeable (Fig. 3e and f). The rod-like and needle-shaped minerals are characteristic of lepidocrocite [11,14]. The results are further confirmed by XRD and Raman spectra analysis in the following sections. Besides, it was observed that the sizes of the minerals formed after aging are increased with aging and up to several micrometers, which evidenced that the corrosion products of nZVI are no longer nanoscale anymore, which is important for the risk assessment of environmental application of nZVI.

The changes in the size and structure of CMC-nZVI nanoparticles in water with aging are shown in Fig. 3A–F. The fresh CMC-nZVI particles appear very well dispersed with particle size in the order of few nanometers (Fig. 3A). After 5 days of aging, the CMC-nZVI nanoparticles were partially oxidized and large blocks of iron oxide were noticeable (Fig. 3B). Lepidocrocite (needle-like material) can be identified in the SEM pattern of CMC-nZVI aged for 15 days and the amounts of which further increased after 30 days of aging (Fig. 3C–F). In comparison with the bare nZVI, it was found that the CMC-nZVI particles have more lepidocrocite crystals when the aging time reaches 30 days. Besides, it was interesting to observe that a bunch of small-sized lepidocrocite was encapsuled by a layer of film in the aged CMC-nZVI (Fig. 3D–F). This may be resulted

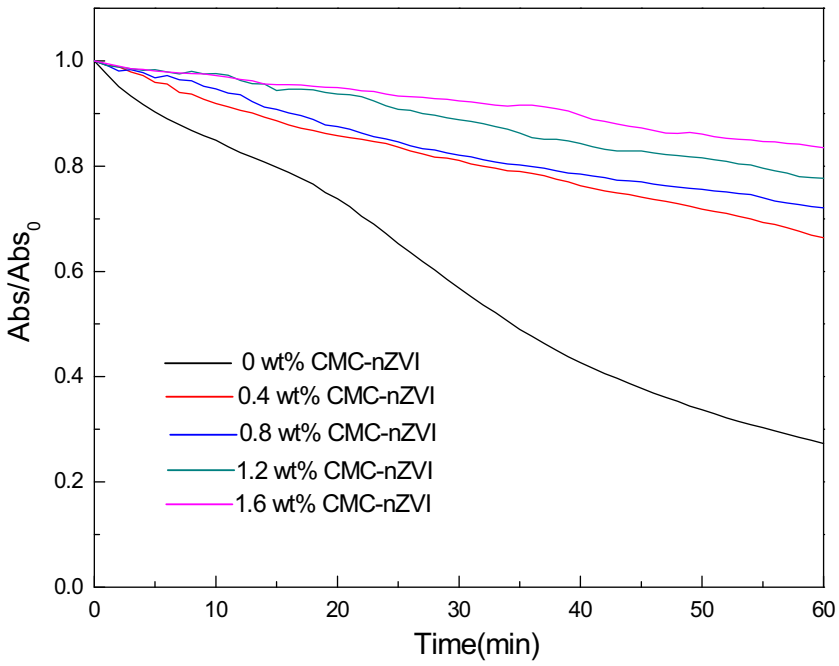

Fig. 1. Changes in relative absorbance over time in sedimentation tests with different CMC-nZVI at a suspension concentration of 500 mg L^{-1}.

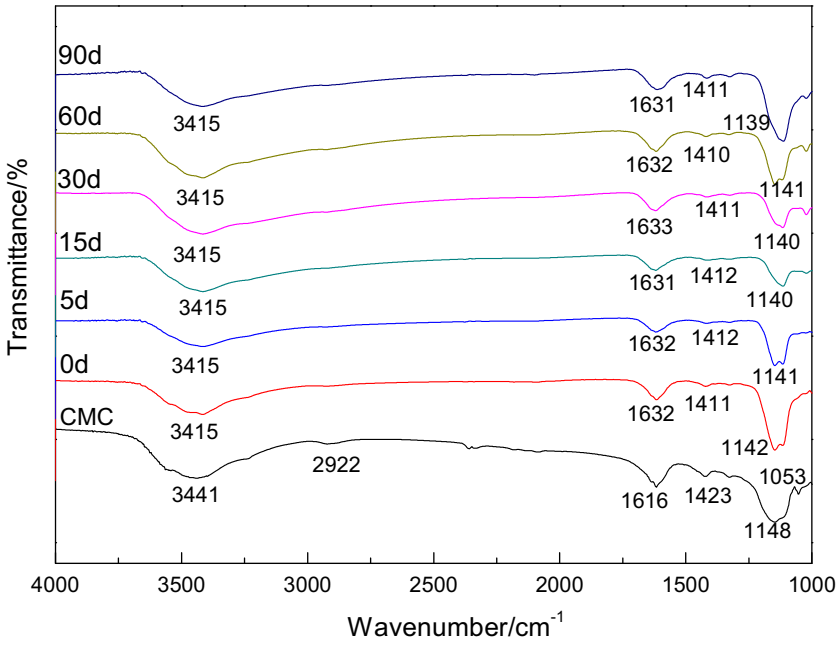

Fig. 2. FTIR analysis of CMC and 0.4 wt% CMC-nZVI aged from 0 day to 90 days in static water.

from the effect of CMC, which inhibited the outward diffusion of dissolved iron into the aqueous phase.

3.4. XRD analysis

The composition evolution of the bare nZVI and CMC-nZVI particles at different CMC loadings (0.4 wt% and 1.2 wt%) were investigated by XRD analysis (Fig. 4). The XRD patterns in Fig. 4a show the composition of the fresh bare nZVI and CMC-nZVI particles. The peaks at $2\theta = 45^\circ$ and 65° should be assigned to Fe(0) [39]. Secondary peak "M" represents the existence of a small amount of iron oxide (magnetite/maghemite), but the magnetite and maghemite peaks are not differentiable by XRD patterns because their lattice parameters are very similar [40]. The other peaks "S" as demonstrated in the XRD pattern of CMC-nZVI are identified to be Na_2SO_4, which is one impurity in the process of CMC synthesis (as shown in XRD pattern of CMC, Fig. 4a).

XRD analysis reveals that the peaks at 2θ of 30.1, 35.4–35.6, 43.4 and 62.5° are credited to magnetite (Fe_3O_4) and/or maghemite (γ-Fe_2O_3) for both nZVI and CMC-nZVI aged for 5 days (Fig. 4b–d). Compared with the fresh nZVI and CMC-nZVI, the peak of Fe^0 in the aged samples became weaker and the intensity of peaks of magnetite and/or maghemite increased. It should be noted that the peak intensity of magnetite and/or maghemite decreased with increasing concentration of CMC from 0 wt% to 1.2 wt%. This indicates the concentration of CMC may determine the extent of oxidation

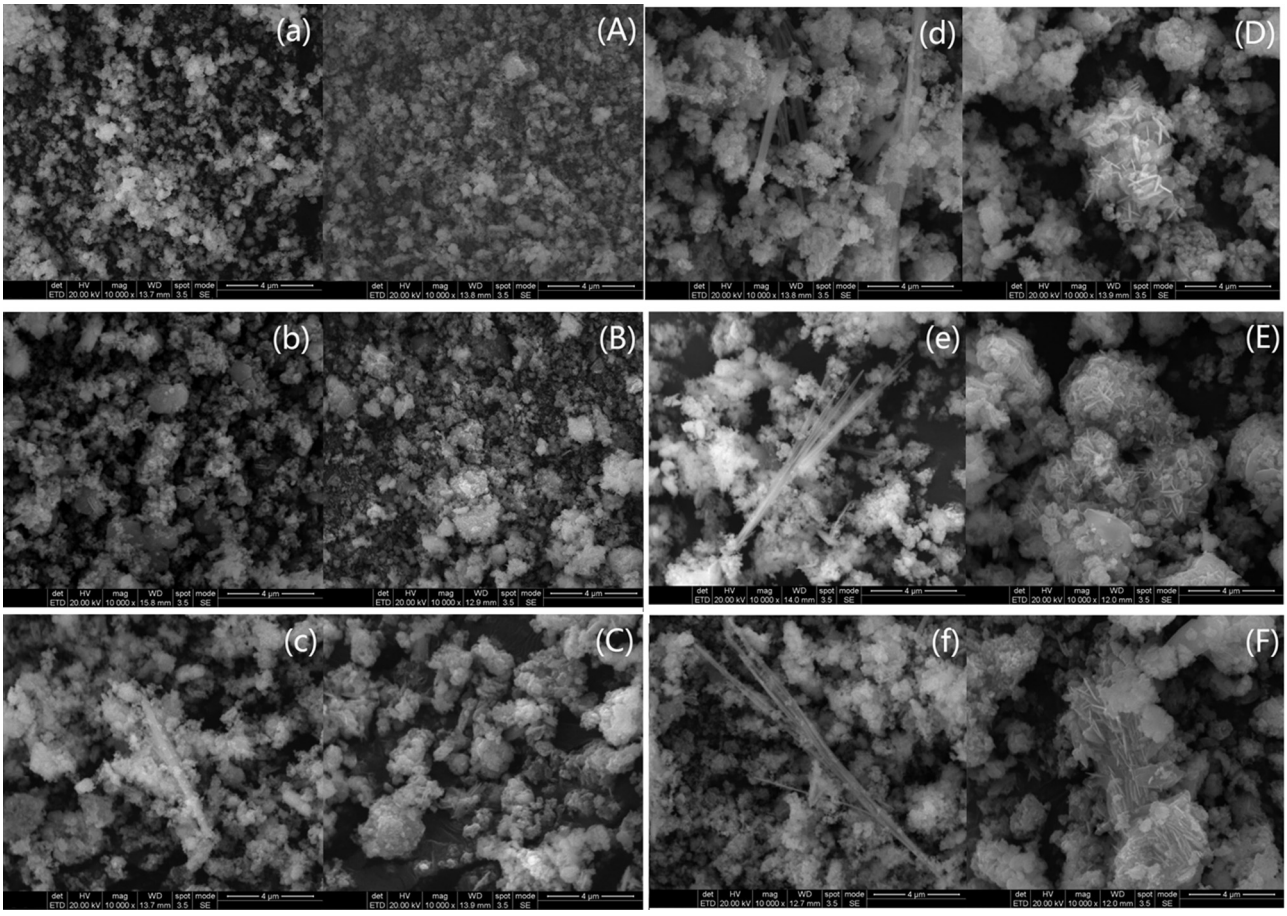

Fig. 3. SEM images of nZVI aged in water from 0 to 90 days: (a) 0 day; (b) 5 days; (c) 15 days; (d) 30 days; (e) 60 days; (f) 90 days; and 0.4 wt% CMC-nZVI aged in water from 0 to 90 days: (A) 0 day;(B) 5 days; (C) 15 days; (D) 30 days; (E) 60 days; (F) 90 days.

of particles at the early stage of aging in static water. He et al. [34] reported that the surface coating could reduce the interaction between the highly reactive surface of the bare nZVI particles and the geochemical conditions of the surrounding media (e.g., DO and water). Peaks observed at 2θ of 14.1, 27.0, 36.3, 38.1 and 58.8 in the 15days

According to the XRD patterns, after 60 days of aging, the magnetite and/or maghemite are the dominant corrosion products for the bare nZVI. However, the corrosion products predominantly feature lepidocrocite and a small quantity of magnetite and/or maghemite for CMC-nZVI. Moreover, more lepidocrocite present in the corrosion products of 1.2 wt% CMC-nZVI than the 0.4 wt% CMC-nZVI. This indicates that the CMC coating could not only influence the extent of oxidation but also the transformation of iron oxides. However, the underlying mechanisms for the different composition evolution w/o the CMC coating were not further investigated and will be the center objective for the future research.

As discussed above, it is concluded that the magnetite or/and maghemite and lepidocrocite were the dominant aging products after aging of nZVI and CMC-nZVI, respectively. Several studies have also reported on the characterization of the corrosion products of nZVI under various conditions [11–13]. However, compositions of the corrosion products varied considerably in different literature, which should be attributable to the difference among iron types (nZVI was produced from nanosized ferrihydrite in this study), contaminant identities, solution compositions, and environmental media. Liu et al. [11] reported that the corrosion products predominantly feature lepidocrocite and a small quantity of magnetite and/or maghemite after 60 days of aging and the longer the aging period, the more lepidocrocites exist in the aged nZVI (synthesized from ferric reduction by $NaBH_4$). The research on corrosion products of As(V) reaction with nZVI (synthesized from ferric reduction by $NaBH_4$) showed the main products were different at varying solution pH [12]. At pH 5, the lepidocrocite was the main corrosion product after 60 days of aging. However, only magnetite or/and maghemite was identified at pH 9 [12]. Greenlee et al. [13] reported that in oxygenated water, nZVI was oxidized primarily to iron oxide-hydroxide lepidocrocite. Therefore, it is suggested that further study should be carried out to examine the aging process of different types of nZVI under the same experimental conditions. This is essential to determine the main factors that influence the corrosion process of nZVI under various environmental conditions [41–43].

3.5. Raman spectroscopy analysis

Raman spectroscopy is especially useful if minerals are to be identified that are poorly defined or that cannot easily be distinguished using other methods (e.g., XRD) [44]. Fig. 5 shows Raman spectra of nZVI and 0.4 wt% CMC-nZVI aged in water. There are mainly five bands observed at 226, 293, 411, 613 and 1328 cm^{-1} for the Raman spectra of nZVI after aging for 5 days (Fig. 5a). The bands coincide with the well-established hematite bands, which are clearly visible at 225, 291, 411, 500, 611 and 1321 cm^{-1} [45]. Similarly, the peaks at 222, 287, 400, 599 and 1300 cm^{-1} for CMC-nZVI are also credited to hematite (Fig. 5b). XRD data show that the oxide shell is mainly composed of magnetite/maghemite after 5 days of aging, which is different from the Raman spectra data. It

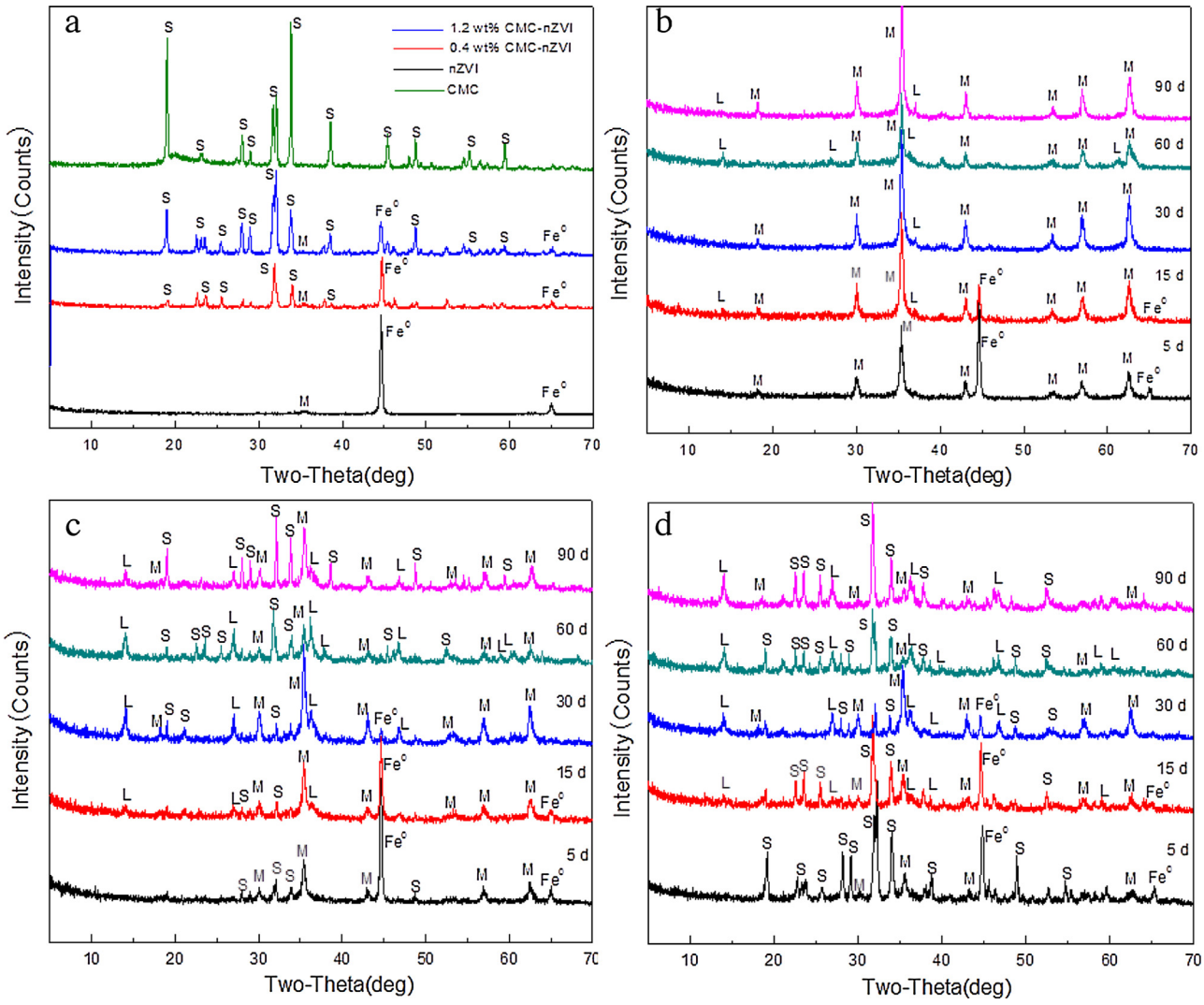

Fig. 4. XRD analysis of nZVI and CMC-nZVI nanoparticles before and after aging: (a) fresh nZVI, CMC-nZVI and CMC; (b) aged nZVI; (c) aged CMC-nZVI (0.4 wt% CMC); (d) aged CMC-nZVI (1.2 wt% CMC). Peaks refer to magnetite/maghemite (Fe_3O_4/γ-Fe_2O_3) (M), (γ-FeOOH)(L), nZVI (Fe^0) and Na_2SO_4(S).

has been reported that laser irradiation causes iron oxyhydroxides to transform into hematite [44]. The Raman bands corresponding to hematite are likely an artifact resulting from the laser induced thermal heating of magnetite. This is evidenced by the absence of hematite in the XRD data. These results were in agreement with those found in the literature [11]. Compared to the CMC-nZVI, the bare nZVI shows a small peak at 245 cm^{-1}, which is assigned to lepidocrocite. The lepidocrocite yields the bands at 250, 348, 379, 528, 650, 1307 cm^{-1} [45]. There is a band at 661 cm^{-1} in addition to other peaks for bare nZVI, which are similar to those observed with CMC-nZVI. It may be the simultaneous existence of maghemite (665, 730 cm^{-1}), magnetite (670 cm^{-1}), and lepidocrocite (650 cm^{-1}). For the samples aged for 15 days and 30 days in static water, both bare nZVI and CMC-nZVI have not much change compared with that aged for 5 days, but the peak at 246 cm^{-1} for nZVI is enhanced and a new peak at 243 cm^{-1} appeared for CMC-nZVI aged for 30 days, which reveals the amount of lepidocrocite is increased. This is consistent with the XRD results.

When the aging time of nZVI and CMC-nZVI was prolonged to 60 days, the Raman patterns show poor shape either in low laser powers or high laser powers, which are probably due to the weak crystal structure of the corrosion products. The peaks at 222, 288, 405 and 607 cm^{-1} for nZVI are also credited to hematite. It can also be observed that the peak of nZVI at 1308 cm^{-1} coincide with lepidocrocite at 1307 cm^{-1}. The results are somewhat different from XRD results, which demonstrate that magnetite and/or maghemite are the major components for iron oxide shell in the aged nZVI. As discussed above, the main reason is that the high power laser irradiation levels may alter the Fe_3O_4 structure with the formation of α-Fe_2O_3 phase [44]. The peak positions of CMC-nZVI aged for 60 days at 249 cm^{-1} and 377 cm^{-1} are in fine agreement with the Raman spectra of lepidocrocite. The small peak at 667 cm^{-1} is ascribed to the low content of magnetite or maghemite. After 90 days of aging, the peaks of aged nZVI are similar to that of 30 days–60 days. However, a new peak is appeared at 261 cm^{-1} for the aged CMC-nZVI for 90 days, which is credited to the combination of feroxyhyte that the standard spectra recorded at 268 cm^{-1} [46]. The transformation from lepidocrocite to feroxyhyte may be occurred in the presence of CMC. Typical Raman peaks of different oxyhydroxides are shown in Table 2.

4. Conclusions and implications

In this study, aging experiments were carried out to assess the long-term compositional and structural evolution of bare nZVI and CMC-coated nZVI. The final corrosion products of nZVI and CMC-

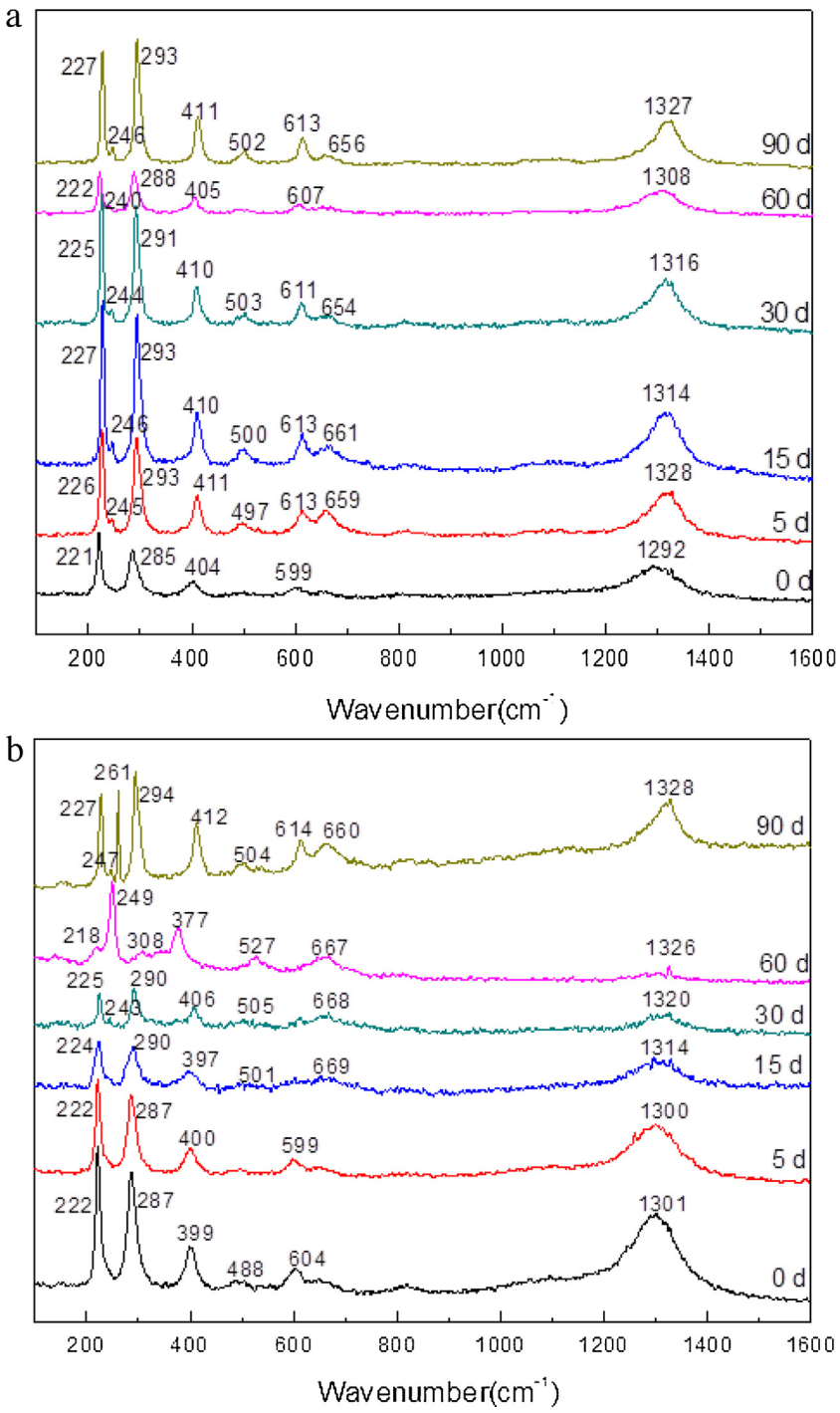

Fig. 5. Raman spectrum of (a) nZVI and (b) 0.4 wt% CMC-nZVI aged from 0 day to 90 days in static water.

Table 2
Raman peaks of iron oxide, hydroxides, and oxyhydroxide for the aging products of nZVI.

Iron oxides	Raman shift (cm^{-1})
Hematite (α-Fe_2O_3)	225,291,411, 500, 611, 1300, 1321
Lepidocrocite (γ-FeOOH)	250, 348, 379, 528, 650,1307
Magnetite (Fe_3O_4)	310, 540, 670
Maghemite (γ-Fe_2O_3)	380, 460, 510, 670, 720
Feroxyhyte (δ-FeOOH)	268, 401, 424,503, 676

nZVI after aging from 0 day to 90 days in the static water were investigated using a combination of FTIR, SEM, XRD and Raman spectra analysis. It is found that the surface coating (i.e., CMC) not merely make nZVI more colloidally stable but also slow down the oxidation rate of the nZVI nanoparticles. FTIR, SEM, XRD and Raman spectra indicate that corrosion products of nZVI and CMC-nZVI vary in both structure and composition. Extended aging leads to the formation of mainly lepidocrocite and magnetite/maghemite. The magnetite and/or maghemite are the dominant corrosion products for bare nZVI, while the corrosion products predominantly feature lepidocrocite for CMC-nZVI. Moreover, the higher loading of CMC in the CMC-nZVI, the more lepidocrocite present in the corrosion products. This indicates that the surface coating may not only influence the extent of iron oxidation but also the transformation of

iron oxides. To improve the mobility and reactivity of nZVI, different types of surface coatings have been employed to modify nZVI in the practical application. Further investigation is thus needed to obtain a fundamental understanding of the long-term fate of nZVI with different types of surface stabilizers. This would enable an accurate assessment of the associated risks before application in the field.

Acknowledgments

This research was supported by the Fundamental Research Funds for the Central Universities, the National Natural Science Foundation of China (51409100, 51521006, 51378190) and the Program for Changjiang Scholars and Innovative Research Team in University (IRT-13R17). The authors also thank the NANOIRON® Company (Czech Republic, EU) for their generous supply of the free nZVI samples.

Appendix A. Supplementary data

Supplementary data associated with this article can be found, in the online version, at http://dx.doi.org/10.1016/j.jhazmat.2016.03.069.

References

[1] Y.P. Sun, X.Q. Li, J. Cao, W.X. Zhang, H.P. Wang, Characterization of zero-valent iron nanoparticles, Adv. Colloid Interface Sci. 120 (2006) 47–56.
[2] J.E. Martin, A.A. Herzing, W. Yan, X.Q. Li, B.E. Koel, C.J. Kiely, W.X. Zhang, Determination of the oxide layer thickness in core-shell zerovalent iron nanoparticles, Langmuir 24 (2008) 4329–4334.
[3] P. Rao, M.S. Mak, T. Liu, K.C. Lai, I.M. Lo, Effects of humic acid on arsenic(V) removal by zero-valent iron from groundwater with special references to corrosion products analyses, Chemosphere 75 (2009) 156–162.
[4] O.X. Leupin, S.J. Hug, Oxidation and removal of arsenic(III) from aerated groundwater by filtration through sand and zero-valent iron, Water Res. 39 (2005) 1729–1740.
[5] S.R. Kanel, D. Nepal, B. Manning, H. Choi, Transport of surface-modified iron nanoparticle in porous media and application to arsenic(III) remediation, J. Nanopart. Res. 9 (2007) 725–735.
[6] Ç. Üzüm, T. Shahwan, A.E. Eroğlu, I. Lieberwirth, T.B. Scott, K.R. Hallam, Application of zero-valent iron nanoparticles for the removal of aqueous Co^{2+} ions under various experimental conditions, Chem. Eng. J. 144 (2008) 213–220.
[7] L.N. Shi, Y.M. Lin, X. Zhang, Z.L. Chen, Synthesis: characterization and kinetics of bentonite supported nZVI for the removal of Cr(VI) from aqueous solution, Chem. Eng. J. 171 (2011) 612–617.
[8] W. Yan, R. Vasic, A.I. Frenkel, B.E. Koel, Intraparticle reduction of arsenite (As(III)) by nanoscale zerovalent iron (nZVI) investigated with in situ X-ray absorption spectroscopy, Environ. Sci. Technol. 46 (2012) 7018–7026.
[9] Y. Su, A.S. Adeleye, Y. Huang, X. Sun, C. Dai, X. Zhou, Y. Zhang, A.A. Keller, Simultaneous removal of cadmium and nitrate in aqueous media by nanoscale zerovalent iron (nZVI) and Au doped nZVI particles, Water Res. 63 (2014) 102–111.
[10] H.R. Dong, G.M. Zeng, C. Zhang, J. Liang, K. Ahmad, P. Xu, X.X. He, M.Y. Lai, Interaction between Cu^{2+} and different types of surface-modified nanoscale zero-valent iron during their transport in porous media, J. Environ. Sci. 32 (2015) 180–188.
[11] A. Liu, J. Liu, W.X. Zhang, Transformation and composition evolution of nanoscale zero valent iron (nZVI) synthesized by borohydride reduction in static water, Chemosphere 119 (2015) 1068–1074.
[12] H. Dong, X. Guan, I.M. Lo, Fate of As(V)-treated nano zero-valent iron: determination of arsenic desorption potential under varying environmental conditions by phosphate extraction, Water Res. 46 (2012) 4071–4080.
[13] L.F. Greenlee, J.D. Torrey, R.L. Amaro, J.M. Shaw, Kinetics of zero valent iron nanoparticle oxidation in oxygenated water, Environ. Sci. Technol. 46 (2012) 12913–12920.
[14] H.S. Kim, T. Kim, J.Y. Ahn, K.Y. Hwang, J.Y. Park, T.T. Lim, I. Hwang, Aging characteristics and reactivity of two types of nanoscale zero-valent iron particles (FeBH and FeH2) in nitrate reduction, Chem. Eng. J. 197 (2012) 16–23.
[15] A. Liu, J. Liu, B. Pan, W.X. Zhang, Formation of lepidocrocite (γ-FeOOH) from oxidation of nanoscale zero-valent iron (nZVI) in oxygenated water, RSC Adv. 4 (2014) 57377–57382.
[16] E. Carpenter, S. Calvin, R. Stroud, V. Harris, Passivated iron as core-shell nanoparticles, Chem. Mater. 15 (2003) 3245–3246.
[17] C.M. Wang, D.R. Baer, L.E. Thomas, J.E. Amonette, J. Antony, Y. Qiang, G. Duscher, Void formation during early stages of passivation: initial oxidation of iron nanoparticles at room temperature, J. Appl. Phys. 98 (2005) 094308.
[18] A. Pratt, L. Lari, O. Hovorka, A. Shah, C. Woffinden, S.P. Tear, C. Binns, R. Kröger, Enhanced oxidation of nanoparticles through strain-mediated ionic transport, Nat. Mater. 13 (2014) 26–30.
[19] M. de Kay Thompson, The reaction between iron and water in the absence of oxygen, Trans. Electrochem. Soc. 78 (1940) 251–257.
[20] B.C. Reinsch, B. Forsberg, R.L. Penn, C.S. Kim, G.V. Lowry, Chemical transformations during aging of zerovalent iron nanoparticles in the presence of common groundwater dissolved constituents, Environ. Sci. Technol. 44 (2010) 3455–3461.
[21] J. Filip, F. Karlický, Z. Marušák, P. Lazar, M. Černík, M. Otyepka, R. Zbořil, Anaerobic reaction of nanoscale zerovalent iron with water: mechanism and kinetics, J. Phys. Chem. C 118 (2014) 13817–13825.
[22] T. Phenrat, N. Saleh, K. Sirk, R.D. Tilton, G.V. Lowry, Aggregation and sedimentation of aqueous nanoscale zerovalent iron dispersions, Environ. Sci. Technol. 41 (2007) 284–290.
[23] Z. Fang, X. Qiu, J. Chen, X. Qiu, Debromination of polybrominated diphenyl ethers by Ni/Fe bimetallic nanoparticles: influencing factors kinetics, and mechanism, J. Hazard. Mater. 185 (2011) 958–969.
[24] F. He, M. Zhang, T. Qian, D. Zhao, Transport of carboxymethyl cellulose stabilized iron nanoparticles in porous media: column experiments and modeling, J. Colloid Interface Sci. 334 (2009) 96–102.
[25] J. Fatisson, S. Ghoshal, N. Tufenkji, Deposition of carboxymethylcellulose-coated zero-valent iron nanoparticles onto silica: roles of solution chemistry and organic molecules, Langmuir 26 (2010) 12832–12840.
[26] F. He, D. Zhao, C. Paul, Field assessment of carboxymethyl cellulose stabilized iron nanoparticles for in situ destruction of chlorinated solvents in source zones, Water Res. 44 (2010) 2360–2370.
[27] T. Raychoudhury, G. Naja, S. Ghoshal, Assessment of transport of two polyelectrolyte-stabilized zero-valent iron nanoparticles in porous media, J. Contam. Hydrol. 118 (2010) 143–151.
[28] A. Tiraferri, K.L. Chen, R. Sethi, M. Elimelech, Reduced aggregation and sedimentation of zero-valent iron nanoparticles in the presence of guar gum, J. Colloid Interface Sci. 324 (2008) 71–79.
[29] B. Schrick, B.W. Hydutsky, J.L. Blough, T.E. Mallouk, Delivery vehicles for zerovalent metal nanoparticles in soil and groundwater, Chem. Mater. 16 (2004) 2187–2193.
[30] H. Dong, I.M. Lo, Influence of humic acid on the colloidal stability of surface-modified nano zero-valent iron, Water Res. 47 (2013) 419–427.
[31] S. Chatterjee, S.R. Lim, S.H. Woo, Removal of Reactive Black 5 by zero-valent iron modified with various surfactants, Chem. Eng. J. 160 (2010) 27–32.
[32] H. Dong, I.M.C. Lo, Transport of surface-modified nano zero-valent iron (SM-NZVI) in saturated porous media: effects of surface stabilizer type subsurface geochemistry, and contaminant loading, Water Air Soil Poll. 225 (2014) 1–12.
[33] T. Phenrat, N. Saleh, K. Sirk, H.J. Kim, R.D. Tilton, G.V. Lowry, Stabilization of aqueous nanoscale zerovalent iron dispersions by anionic polyelectrolytes: adsorbed anionic polyelectrolyte layer properties and their effect on aggregation and sedimentation, J. Nanopart. Res. 10 (2008) 795–814.
[34] F. He, D. Zhao, J. Liu, C.B. Roberts, Stabilization of Fe–Pd nanoparticles with sodium carboxymethyl cellulose for enhanced transport and dechlorination of trichloroethylene in soil and groundwater, Ind. Eng. Chem. Res. 46 (2007) 29–34.
[35] R.L. Johnson, J.T. Nurmi, G.S. O'Brien Johnson, D. Fan, R.L. O'Brien Johnson, Z. Shi, A.J. Salter-Blanc, P.G. Tratnyek, G.V. Lowry, Field-scale transport and transformation of carboxymethylcellulose-stabilized nano zero-valent iron, Environ. Sci. Technol. 47 (2013) 1573–1580.
[36] T. Phenrat, H.J. Kim, F. Fagerlund, T. Illangasekare, R.D. Tilton, G.V. Lowry, Particle size distribution concentration, and magnetic attraction affect transport of polymer-modified Fe^0 nanoparticles in sand columns, Environ. Sci. Technol. 43 (2009) 5079–5085.
[37] N. Saleh, H.J. Kim, T. Phenrat, K. Matyjaszewski, R.D. Tilton, G.V. Lowry, Ionic strength and composition affect the mobility of surface-modified FeO nanoparticles in water-saturated sand columns, Environ. Sci. Technol. 42 (2008) 3349–3355.
[38] A. Cabot, V.F. Puntes, E. Shevchenko, Y. Yin, L. Balcells, M.A. Marcus, S.M. Hughes, A.P. Alivisatos, Vacancy coalescence during oxidation of iron nanoparticles, J. Am. Chem. Soc. 129 (2007) 10358–10360.
[39] J.T. Nurmi, P.G. Tratnyek, V. Sarathy, D.R. Baer, J.E. Amonette, K. Pecher, C. Wang, J.C. Linehan, D.W. Matson, R.L. Penn, M.D. Driessen, Characterization and properties of metallic iron nanoparticles: spectroscopy electrochemistry, and kinetics, Environ. Sci. Technol. 39 (2005) 1221–1230.
[40] Q. Wang, S. Snyder, J. Kim, H. Choi, Aqueous ethanol modified nanoscale zerovalent iron in bromate reduction: synthesis characterization, and reactivity, Environ. Sci. Technol. 43 (2009) 3292–3299.
[41] X.H. Guan, Y.K. Sun, H.J. Qin, J.X. Li, I.M.C. Lo, D. He, H.R. Dong, The limitations of applying zero-valent iron technology in contaminants sequestration and the corresponding countermeasures: the development in zero-valent iron technology in the last two decades (1994–2014), Water Res. 75 (2015) 224–248.
[42] P. Feng, X.H. Guan, Y.K. Sun, W. Choi, H.J. Qin, J.M. Wang, J.L. Qiao, L.N. Li, Weak magnetic field accelerates chromate removal by zero-valent iron, J. Environ. Sci. 31 (2015) 175–183.

[43] H.R. Dong, Q. He, G.M. Zeng, L. Tang, C. Zhang, Y.K. Xie, Y.L. Zeng, F. Zhao, Y.N. Wu, Chromate removal by surface-modified nanoscale zero-valent iron: effect of different surface coatings and water chemistry, J. Colloid Interface Sci. 471 (2016) 7–13.
[44] M. Hanesch, Raman spectroscopy of iron oxides and (oxy)hydroxides at low laser power and possible applications in environmental magnetic studies, Geophys. J. Int. 177 (2009) 941–948.
[45] S.J. Oh, D. Cook, H. Townsend, Characterization of iron oxides commonly formed as corrosion products on steel, Hyperfine Interact. 112 (1998) 59–66.
[46] M.K. Nieuwoudt, J.D. Comins, I. Cukrowski, The growth of the passive film on iron in 0.05 M NaOH studied in situ by Raman micro-spectroscopy and electrochemical polarisation. Part I: near-resonance enhancement of the Raman spectra of iron oxide and oxyhydroxide compounds, J. Raman Spectrosc. 42 (2011) 1335–1339.